

Three Hot-Jupiters on the upper edge of the mass-radius distribution: WASP-177, WASP-181 and WASP-183

Oliver D. Turner,^{1*} D.R. Anderson,² K. Barkaoui,^{3,4} F. Bouchy,¹ Z. Benkhaldoun⁴
 D.J.A. Brown,^{5,6} A. Burdanov,³ A. Collier Cameron,⁷ E. Ducrot,³ M. Gillon,³
 C. Hellier,² E. Jehin,³ M. Lendl,^{8,1} P.F.L. Maxted,² L.D. Nielsen,¹ F. Pepe,¹
 D. Pollacco,^{5,6} F.J. Pozuelos,³ D. Queloz,^{1,9} D. Ségransan,¹ B. Smalley,²
 A.H.M.J. Triaud,¹⁰ S. Udry¹, and R.G. West^{5,6}

¹Observatoire de Genève, Université de Genève, 51 Chemin des Maillettes, 1290 Sauverny, Switzerland

²Astrophysics Group, Keele University, Staffordshire ST5 5BG, UK

³Space sciences, Technologies and Astrophysics Research (STAR) Institute, Université de Liège, Liège 1, Belgium

⁴Oukaimeden Observatory, High Energy Physics and Astrophysics Laboratory, Cadi Ayyad University, Marrakech, Morocco

⁵Department of Physics, University of Warwick, Coventry CV4 7AL, UK

⁶Centre for Exoplanets and Habitability, University of Warwick, Gibbet Hill Road, Coventry CV4 7AL, UK

⁷SUPA, School of Physics and Astronomy, University of St. Andrews, North Haugh, Fife KY16 9SS, UK

⁸Space Research Institute, Austrian Academy of Sciences, Schmiedlstr. 6, A-8042 Graz, Austria

⁹Cavendish Laboratory, J J Thomson Avenue, Cambridge CB3 0HE, UK

¹⁰School of Physics & Astronomy, University of Birmingham, Edgbaston, Birmingham, B15 2TT, UK

Accepted XXX. Received YYY; in original form ZZZ

ABSTRACT

We present the discovery of 3 transiting planets from the WASP survey, two hot-Jupiters: WASP-177 b ($\sim 0.5 M_{\text{Jup}}$, $\sim 1.6 R_{\text{Jup}}$) in a 3.07-d orbit of a $V = 12.6$ K2 star, WASP-183 b ($\sim 0.5 M_{\text{Jup}}$, $\sim 1.5 R_{\text{Jup}}$) in a 4.11-d orbit of a $V = 12.8$ G9/K0 star; and one hot-Saturn planet WASP-181 b ($\sim 0.3 M_{\text{Jup}}$, $\sim 1.2 R_{\text{Jup}}$) in a 4.52-d orbit of a $V = 12.9$ G2 star. Each planet is close to the upper bound of mass-radius space and has a scaled semi-major axis, a/R_* , between 9.6 and 12.1. These lie in the transition between systems that tend to be in orbits that are well aligned with their host-star’s spin and those that show a higher dispersion.

Key words: planets and satellites: detection – planets and satellites: individual: WASP-177b – planets and satellites: individual: WASP-181b – planets and satellites: individual: WASP-183b

1 INTRODUCTION

Since the beginning of the project the Wide Angle Search for Planets (WASP; Pollacco et al. 2006) survey has discovered nearly 190 transiting, close-in, giant exoplanets. As they transit their host stars their bulk properties, mass and radius, can be determined relatively easily. Their transits allow for deeper characterisation that has led to the discovery of multiple chemical and molecular species in their atmospheres (Birkby et al. 2013; de Kok et al. 2013; Wyttenbach et al. 2017; Hoeijmakers et al. 2018) and the observation of planetary winds (Brogi et al. 2016).

Close-in exoplanets can also provide information on the

formation and migration mechanisms of solar systems. It is expected that hot-Jupiter exoplanets initially form much further from their stars than where we detect them today. Therefore some mechanism must cause this migration. There are two proposed pathways, high eccentricity migration or disk migration. In the former some mechanism e.g. Kozai cycles (Wu & Murray 2003; Armitage 2013) or planet-planet scattering (Rasio & Ford 1996; Weidenschilling & Marzari 1996), forces the cold Jupiter into a highly eccentric orbit which then is tidally circularised via interaction with the star. During this kind of migration it is possible for the planet orbital axis to become mis-aligned with the stellar spin axis (Fabrycky & Tremaine 2007). In the latter mechanism the planet loses angular momentum via interaction with the stellar disk during formation and migrates inward

* E-mail: oliver.turner@unige.ch

(Goldreich & Tremaine 1980). This is expected to preserve the initial spin-orbit alignment (Marzari & Nelson 2009), though work is being done to investigate the production of mis-aligned planets due to inclined protoplanetary discs (Xiang-Gruess & Kroupa 2017).

The alignment between the stellar rotation axis and planet orbit can be investigated with the Rossiter-McLaughlin (RM) technique (Rossiter 1924; McLaughlin 1924; Triaud et al. 2010, etc.). These observations have shown a general trend for systems orbiting cool stars (with $T_{\text{eff}} < 6250\text{K}$; Albrecht et al. 2012; Anderson et al. 2015b) to be more well aligned than systems orbiting hotter stars. Tides are also expected to play a role. In cool star systems, those with smaller scaled semi-major axes, a/R_* , tend to be more often well aligned than those with larger a/R_* . Though this picture is far from clear as there seems to be evidence for the hot/cool alignment disparity holding even for systems with large separations or low mass planets meaning tidal effects should be minimal (Mazeh et al. 2015) casting tidal realignment into doubt (see also the discussion of Dai & Winn 2017).

In this paper we present the discovery of three systems at the upper edge of the mass-radius envelop of hot-giants that could be useful probes of tidal re-alignment.

2 OBSERVATIONS

Each of these planets was initially flagged as a candidate in data taken with both WASP arrays located at Roque de los Muchachos Observatory on La Palma and at the South African Astronomical Observatory (SAAO). The data were searched for periodic signals using a BLS method as per Collier Cameron et al. (2006, 2007). The survey itself is described in more detail by Pollacco et al. (2006).

In order to confirm the planetary nature of the signals radial velocity (RV) data were obtained with the CORALIE spectrograph on the 1.2-m Swiss telescope at La Silla, Chile (Queloz et al. 2000). Additional photometry was acquired using EulerCam (Lendl et al. 2012, also on the 1.2-m Swiss) and the two 0.6-m TRAPPIST telescopes (Gillon et al. 2011; Jehin et al. 2011), based at La Silla and Oukaimeden Observatory in Morocco (Gillon et al. 2017; Barkaoui et al. 2018).

Due to the low masses of WASP-181 b and WASP-183 b, we also acquired HARPS data¹. These observations are summarised in Table 1. The TRAPPIST data from 2018-08-13 contain a meridian flip at BJD = 2458344.5639. During analysis the data were partitioned at this point and modeled as two datasets.

Figures ??, 1 and 2 show the phase folded discovery and follow-up data. The RVs exhibit signals in phase with those found in the transit data and are consistent with companion objects of planetary mass. We checked for correlation between the RV variation and the bisector spans, see Fig.3. We find no strong correlation and so further exclude the possibility that these objects are transit mimics.

¹ These observations were made as part of the programs Anderson:0100.C-0847(A) and Nielsen:0102.C-0414(A).

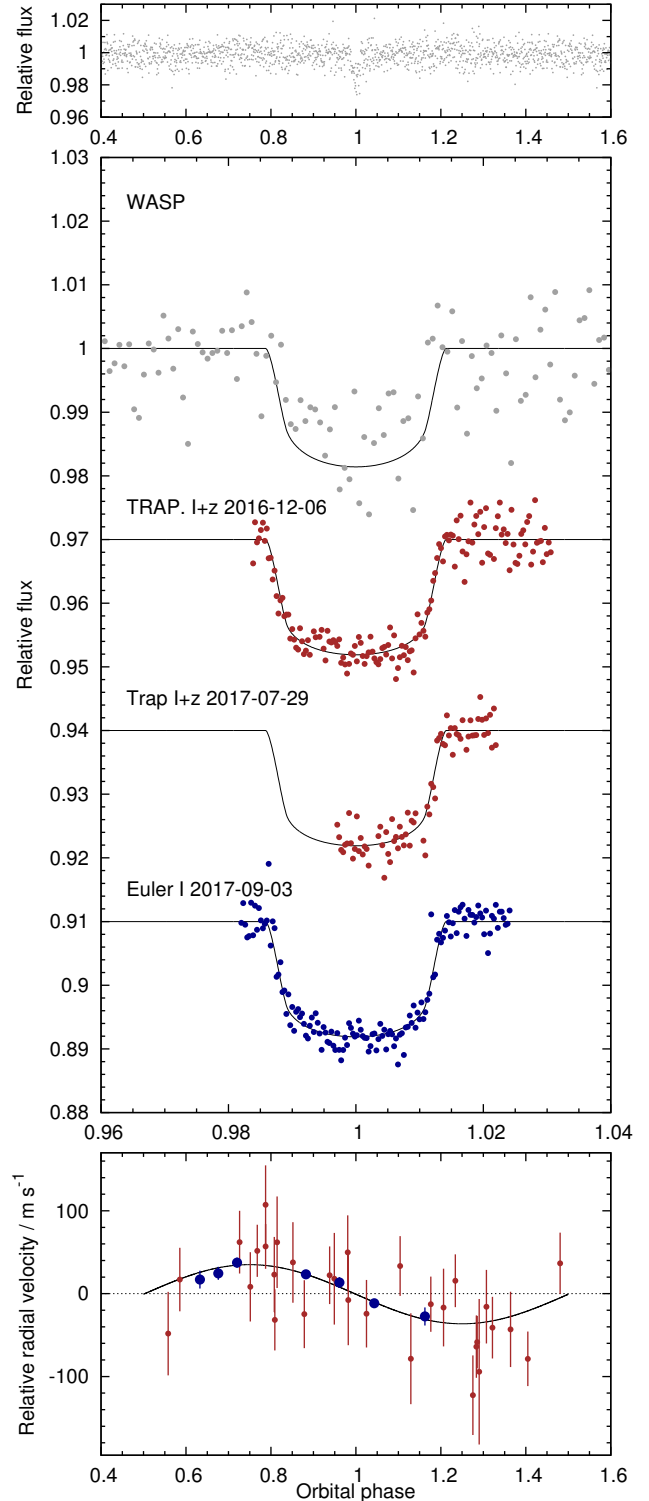


Figure 1. As for Fig.?? for the WASP-181 system. CORALIE data in bottom figure are small (red) while HARPS data are larger (blue) symbols.

Table 1. Observations of WASP-177, WASP-181 and WASP-183.

Date	Source	N.Obs. Filter
WASP-177		
2008 Jul–2010 Oct	WASP (North)	16 169
2008 Jun–2009 Oct	WASP (South)	10 825
2016 Aug–2018 Sep	CORALIE	26
2017 Jul 25	TRAPPIST-North	I+z
2017 Oct 19	EulerCam	B
2018 Jul 13	EulerCam	V
2018 Aug 13	TRAPPIST-North ^a	I+z
WASP-181		
2008 Sep–2010 Dec	WASP (North)	12 938
2008 Jul–2009 Aug	WASP (South)	9 059
2016 Jan–2017 Dec	CORALIE	31
2018 Oct–2019 Jan	HARPS	7
2016 Dec 06	TRAPPIST-South	I+z
2017 Jul 29	TRAPPIST-North	I+z
2017 Sep 03	EulerCam	I _c
WASP-183		
2008 Feb–2011 Mar	WASP (North)	13 733
2009 Jan–2010 May	WASP (South)	10 789
2015 May–2018 Jul	CORALIE	16
2018 Mar	HARPS	4
2018 Feb 24	TRAPPIST-North	I+z

^a Meridian flip at BJD 2458344.5639.

3 ANALYSIS

3.1 Stellar Parameters

To obtain the stellar parameters effective temperature, T_{eff} , metallicity, [Fe/H], and surface gravity, $\log g$, we followed the method of Giles et al. (2018a,b) using iSpec (Blanco-Cuaresma et al. 2014b). To do this we corrected each spectrum for the computed RV shift, cleaned them of cosmic ray strikes and convolved them to a spectral resolution, R , of 47 000. Then, ignoring areas typically affected by telluric lines we used the synthetic spectral fitting technique to derive the stellar parameters. Via iSpec we used SPECTRUM (Gray & Corbally 1994) as the radiative transfer code with atomic data from VALD (Kupka et al. 2011), a line selection based on a $R \sim 47\,000$ solar spectrum (Blanco-Cuaresma et al. 2016, 2017) and the MARCS model atmospheres Gustafsson et al. (2008) in the wavelength range 480- to 680-nm. We increased the uncertainties in these parameters by adding the dispersion found by analysing the *Gaia* benchmark stars with iSpec as per Blanco-Cuaresma et al. (2014a); Jofré et al. (2014); Heiter et al. (2015).

We determined the stellar density from an initial fit to the lightcurves and then used it along with the T_{eff} and metallicity to determine stellar masses, for later use in the joint analysis, and the stellar ages with the Bayesian stellar evolution code BAGEMASS (Maxted et al. 2015). The resulting parameters are presented in the top part of Table 3 and the corresponding isochrons/evolutionary tracks are shown in Fig 4.

BAGEMASS uses an MCMC with a densely sampled

grid of stellar models to compute stellar masses and ages. There are three usable grids with differing mixing length parameters, α_{MLT} , and helium enhancement. The default values of these are $\alpha_{\text{MLT}} = 1.78$ and no He-enhancement. We used the BAGEMASS default parameters to model WASP-177 and WASP-181 but found that they did not fit WASP-183 very well. This is likely because WASP-183 is among the $\sim 3\%$ of the K-dwarf population that are larger than models would predict (Spada et al. 2013). To account for this we follow the method of Maxted et al. (2015) in the case of Qatar-2 and use the grid provided by BAGEMASS with $\alpha_{\text{MLT}} = 1.5$. This results in a much improved fit to the observed density and temperature. We find that the resulting mass estimate is unaffected.

3.2 System parameters

To determine the system parameters we modeled the discovery and follow-up data together using the most recent version of the Markov-Chain Monte Carlo (MCMC) code described in detail in Collier Cameron et al. (2007) and Anderson et al. (2015a). We modeled the transit lightcurves using the models of Mandel & Agol (2002) with the 4 parameter limb darkening law of Claret (2000, 2004).

In brief, the models were initialised using the period, P , epoch, T_0 , transit depth, $(R_p/R_s)^2$, transit duration, T_{14} , and impact parameter, b , output by the BLS search of each discovery lightcurve. The spectroscopic stellar effective temperature, T_{eff} , and metallicity, [Fe/H], were used initially to estimate the stellar mass using the updated Torres mass calibration by Southworth (2011). To explore the effect of limb-darkening we extracted tables of limb-darkening parameters in each photometric band used for each star. They were extracted for a range of effective temperatures while keeping the stellar metallicity and surface gravity constant. The values used were perturbed during the MCMC via $T_{\text{L-D}}$, the ‘limb-darkening temperature’, which has a mean and standard deviation corresponding to the spectroscopic T_{eff} and its uncertainty.

At each step of the MCMC each of these values are perturbed and the models are re-fit. These new proposed parameters are then accepted if the χ^2 of the fit is better or accepted with a probability proportional to $\exp(-\Delta\chi^2)$ if the χ^2 of the fit is worse.

In the final MCMCs, in place of using the Torres relation to determine a mass, we provided the value given by BAGEMASS. The code then drew values at each step from a Gaussian with a mean and standard deviation given by the value and its uncertainty respectively. Due to the lack of good quality follow-up photometry we imposed a similar prior on the radius of the star WASP-183 using the *Gaia* parallax. Lacking a complete, good quality follow-up lightcurve can lead to a poor determination of, ΔF , T_{14} and b which we use to calculate the R_*/a . This in turn results in a poorer determination of R_* , R_p and other parameters that depend upon them.

In this way we also explored models allowing for eccentric orbits and the potential for linear drifts in the RVs. There was no strong evidence supporting either scenario so we present the system solutions corresponding to circular orbits (Anderson et al. 2012) with no trends due to unseen

Table 2. Periodogram analysis for WASP lightcurves of WASP-177.

WASP Inst.	Dates JD-2450000	Period P_{rot} (d)	Amp (mag.)	FAP	Notes
North	4656-4767	7.569	0.005	0.0017	P/2
North	5026-5131	7.528	0.006	<0.0001	P/2
North	5387-5498	14.860	0.004	<0.0001	
South	4622-4764	14.330	0.005	0.0007	
South	4984-5129	7.456	0.006	<0.0001	P/2

companions. The parameters derived by these fits can be found in the lower part of Table 3.

3.3 Rotational modulation

We checked the WASP lightcurves of the three stars for rotational modulation that could be caused by star spots using the method described by Maxted et al. (2011). The transits were fit with a simple model and removed. We performed the search over 16384 frequencies ranging from 0 to 1 cycles/day. Due to the limited lifetime and variable distribution of star spots this modulation is not expected to be coherent over long periods of time. As such, we modeled each season of data from each camera individually. WASP-181 and WASP-183 show no significant modulation, with an upper limit on the amplitude of 2- and 3-mmag respectively.

However, WASP-177 was found to exhibit modulation consistent with a rotational period, $P_{\text{rot}} = 14.86 \pm 0.14$ days and amplitude of 5 ± 1 mmag. The results of this analysis for each camera and season of data is shown in Table 2. Fig. 5 shows the periodograms of the fits and the discovery lightcurves phase-folded on the corresponding period of modulation. Three of the datasets exhibit $P_{\text{rot}} \sim 7$ -days while the other two exhibit $P_{\text{rot}} \sim 14$ -days. We interpret the ~ 7 -day signals as a harmonic of the longer ~ 14 -day signal as it is more easy for multiple active regions to produce a ~ 7 -day signal when the true period is ~ 14 -days than vice versa. Using this rotational period and our value for the stellar radius we find a stellar rotational velocity of, $v_* = 2.9 \pm 0.2$ km/s. When compared to the projected equatorial spin velocity we find a stellar inclination to our line of sight of $38 \pm 25^\circ$ which suggests that WASP-177 b could be quite mis-aligned.

4 DISCUSSION

Our joint analysis shows that in this ensemble we have two large sub-Jupiter mass planets: WASP-177 b ($\sim 0.5 M_{\text{Jup}}$, $\sim 1.6 R_{\text{Jup}}$) and WASP-183 b ($\sim 0.5 M_{\text{Jup}}$, $\sim 1.5 R_{\text{Jup}}$) orbiting old stars. The third planet, WASP-181 b, is a large Saturn mass planet ($\sim 0.3 M_{\text{Jup}}$, $\sim 1.2 R_{\text{Jup}}$). According to the analysis with BAGEMASS, WASP-177 and WASP-183 are both at the latter end of the main sequence explaining their slightly larger radii for stars of their spectral class; a 9.7 ± 3.9 Gyr K2 and 14.9 ± 1.7 Gyr G9/K0 respectively. WASP-183 is particularly noteworthy as its advanced age makes it one of the oldest stars known to host a transiting planet (see Fig. 6). Though, WASP-183 appears to be subject to the K-dwarf radius anomaly, making this determination less clear.

Meanwhile, WASP-181 is a relatively young, standard example of a G2 star.

We compared the stellar radii derived from our MCMC to those we can calculate using the Gaia DR2 parallaxes (Luri et al. 2018; Gaia Collaboration et al. 2018), with the correction from Stassun & Torres (2018), and stellar angular radii from the infra-red flux fitting method (IRFM) these radii, with reddening accounted for by the use of dust maps (Schlafly & Finkbeiner 2011). We find good agreement and present a summary in table 4.

All three planets occupy the upper edge of the mass-radius distribution, seen in Fig 7. WASP-181 b is amongst the group of the largest planets for an object of its mass. While its mass is not as well determined as the other two, further HARPS observations will help to refine this. WASP-177 b and WASP-183 b do lie above the bulk of the distribution, especially when compared to other objects with mass determinations of 10% precision or better. However, it is difficult to say how exceptional they are as a precise radius determination has proven difficult for them both. The transit of WASP-177 b is grazing and the transit of WASP-183 b, in addition to being grazing, lacks a full high precision follow-up lightcurve to refine the transit shape. We anticipate that *TESS* observations could soon solve the latter problem; the long cadence data would capture roughly 24 in transit points with a predicted precision from the *ticgen* tool of better than 1000 ppm in each 30-minute observation.

We used the the values derived for planet equilibrium temperature, T_{eq} , and surface gravity, g , along with Boltzmann's constant, k , and the atmospheric mean molecular mass, μ , to estimate the scale heights, H , of these planets as:

$$H = \frac{kT_{\text{eq}}}{g\mu} \quad (1)$$

assuming an isothermal, hydrogen dominated atmosphere. The resulting scale heights were; 790 ± 320 km, 770 ± 200 km, 696 ± 464 km for WASP-177 b, WASP-181 b and WASP-183 b respectively. These translate to transit depth variations of just under 300 ppm for WASP-177 and WASP-181 and ~ 300 ppm for WASP-183. If we account for the K-band flux and scale in the same way as Anderson et al. (2017), we get atmospheric signals of; 70, 41 and 60. In reality, we can expect this metric to be an over estimate of detectability for WASP-177 b and WASP-183 b as the grazing nature of their transits reduces the impact of the atmospheric signal further. For comparison we used the same metric on other planets with atmospheric detections: water has been detected in the atmospheres of both WASP-12 b (Kreidberg et al. 2015; signal ~ 93) and WASP-43 b (Kreidberg et al. 2014; signal ~ 74); titanium oxide has been detected in the atmosphere of WASP-19 b (Sedaghati et al. 2017; signal ~ 83); sodium and potassium have both been detected in the atmosphere of WASP-103 b (Lendl et al. 2017; signal ~ 37). While not ideal targets, this suggests such detections may be possible.

Investigation into any eccentricity or long-period massive companions in these systems has not yielded anything convincing. All of the orbits are circular, with the 2σ upper limits quoted in Table 3. As for long term trends, WASP-177 shows the possibility of a very low significance ($\sim 1.5\sigma$) drift

Table 3. System parameters

Parameter	Symbol (Unit)	WASP-177	WASP-181	WASP-183
1SWASP ID	–	J221911.19-015004.7	J014710.37+030759.0	J105509.36-004413.7
Right ascension	(h:m:s)	22:19:11.19	01:47:10.37	10:55:09.36
Declination	(°:′:″)	-01:50:04.7	+03:07:59.0	-00:44:13.7
V magnitude	–	12.58	12.91	12.76
Spectral type ^a	–	K2	G2	G9/K0
Stellar effective temperature	T_{eff} (K)	5017 ± 70	5839 ± 70	5313 ± 72
Stellar surface gravity	$\log(g)$ (cgs)	4.49 ± 0.07	4.38 ± 0.08	4.25 ± 0.09
Stellar metallicity	[Fe/H] (dex)	0.25 ± 0.04	0.09 ± 0.04	-0.31 ± 0.04
Projected equatorial spin velocity	$V_* \sin I_*$ (km/s)	1.8 ± 1.0	3.3 ± 0.9	1.0 ± 1.0
Stellar macro-turbulent velocity ^b	V_{mac} (km/s)	2.7	3.3	2.8
Stellar age	(Gyr)	9.7 ± 3.9	2.5 ± 1.7	14.9 ± 1.7
Distance ^c	(pc)	178 ± 2	443 ± 8	328 ± 4
Period	P (d)	3.071722 ± 0.000001	4.5195064 ± 0.0000034	4.1117771 ± 0.0000051
Transit Epoch	$T_0 - 2450000$	7994.37140 ± 0.00028	7747.66681 ± 0.00035	7796.1845 ± 0.0024
Transit Duration	T_{14} (d)	0.0672 ± 0.0013	0.1277 ± 0.0015	0.084 ± 0.005
Scaled Semi-major Axis	a/R_s	$9.61^{+0.42}_{-0.53}$	12.09 ± 0.54	11.44 ± 0.54
Transit Depth	$(R_p/R_s)^2$	$0.0185^{+0.0035}_{-0.0014}$	0.01590 ± 0.00038	$0.0226^{+0.0060}_{-0.0036}$
Impact Parameter	b	$0.980^{+0.092}_{-0.060}$	$0.34^{+0.10}_{-0.15}$	$0.916^{+0.163}_{-0.091}$
Orbital Inclination	i (°)	$84.14^{+0.66}_{-0.83}$	$88.38^{+0.76}_{-0.59}$	$85.37^{+0.61}_{-0.88}$
Systemic Velocity	γ (kms ⁻¹)	-7.1434 ± 0.0041	-8.5489 ± 0.0072	68.709 ± 0.012
Semi-amplitude	K_1 (ms ⁻¹)	77.3 ± 5.2	35.7 ± 3.9	74.8 ± 6.6
Semi-major Axis	a (au)	0.03957 ± 0.00058	0.05427 ± 0.00069	0.04632 ± 0.00075
Stellar Mass	M_s (M_\odot)	0.876 ± 0.038	1.04 ± 0.04	0.784 ± 0.038
Stellar Radius	R_s (R_\odot)	0.885 ± 0.046	0.965 ± 0.043	0.871 ± 0.038
Stellar Density	ρ_s (ρ_\odot)	$1.26^{+0.23}_{-0.15}$	1.16 ± 0.15	1.19 ± 0.17
Stellar Surface Gravity	$\log(g_s)$ (cgs)	$4.486^{+0.049}_{-0.037}$	4.487 ± 0.039	4.452 ± 0.043
Limb-darkening Temperature	$T_{\text{L-D}}$ (K)	5012 ± 69	5835 ± 70	5313 ± 72
Stellar Metallicity	[Fe/H]	0 ± 0	0 ± 0	0 ± 0
Planet Mass	M_p (M_{Jup})	0.508 ± 0.038	0.299 ± 0.034	0.502 ± 0.047
Planet Radius	R_p (R_{Jup})	$1.58^{+0.66}_{-0.36}$	$1.184^{+0.071}_{-0.059}$	$1.47^{+0.94}_{-0.33}$
Planet Density	ρ_p (ρ_{Jup})	$0.130^{+0.133}_{-0.085}$	0.179 ± 0.033	$0.16^{+0.18}_{-0.12}$
Planet Surface	$\log(g_p)$ (cgs)	$2.67^{+0.22}_{-0.31}$	2.686 ± 0.065	$2.72^{+0.22}_{-0.43}$
Planet Equilibrium Temperature ^d	T_{eq} (K)	1142 ± 32	1186^{+32}_{-26}	1111 ± 30

^a Spectral type estimated by comparison of T_{eff} to the table in Gray (2008).

^b Derived via the method of Doyle et al. (2014).

^c From Gaia DR2 Gaia Collaboration et al. (2016, 2018); Luri et al. (2018).

^d Assuming 0 albedo and complete redistribution of heat.

Table 4. Comparison of stellar radii output by the MCMC analysis with radii derived from Gaia DR2.

Radius source	WASP-177	WASP-181	WASP-183
MCMC	0.885 ± 0.046	0.965 ± 0.043	0.871 ± 0.038
Gaia parallax + IRFM (Corrected)	0.80 ± 0.04	0.97 ± 0.06	0.87 ± 0.04
Gaia parallax + IRFM (Uncorrected)	0.81 ± 0.04	1.01 ± 0.05	0.89 ± 0.04
Reddening	0.072	0.023	0.04

with $\delta\gamma/\delta t$ of $(-2.4 \pm 1.6) \times 10^{-5}$ km/s/d. Neither WASP-181 nor WASP-183 show significant drifts with $\delta\gamma/\delta t$ of $(1.2 \pm 4.0) \times 10^{-5}$ km/s/d and $(-1.9 \pm 5.1) \times 10^{-5}$ km/s/d respectively.

Finally, these systems do present interesting targets for the investigation of the observed spin-orbit mis-alignment distribution (Albrecht et al. 2012; Anderson et al. 2015b).

All of the stellar hosts fall into the “cool” regime of Albrecht et al. (2012) and despite their short periods have scaled semi-major axes, a/R_* , above 8. They are therefore above the empirical boundary noted by Dai & Winn (2017) as the transition region where systems with cooler stars show more tendency to be mis-aligned. Since the study in 2017 the number of systems with obliquity measurements has increased. Most of the cool-star systems with a/R_* above 8 are well aligned, see Fig 8.

We estimated the alignment time-scale for each system using Eq.4 of Albrecht et al. (2012) as was done for WASP-117 (Lendl et al. 2014). These time-scales, along with the mass of the convective zone, M_{cz} , are shown in Tab 5. In each case, the time-scale for realignment is much longer than the

Table 5. Convective zone masses and estimated time-scales for realignment of systems in this paper.

Star	M_{cz}^a (M_{\odot})	τ (Gyr)
WASP-177	$10^{-1.3}$	120
WASP-181	$10^{-1.7}$	7500
WASP-183	$10^{-1.4}$	200

^a Derived from [Pinsonneault et al. \(2001\)](#).

ages of the systems. Therefore, we would expect the initial state of alignment of the systems to have been preserved. We have estimated the inclination of WASP-177 to be $38 \pm 25^\circ$ and so may expect it to join only 12 systems with a/R_* < 15 that show mis-alignment this makes it a potentially important diagnostic in determining the factors that cause or preserve mis-alignment.

We calculate that the amplitude of the RM effect will be greatest for WASP-181 at $\sim 50 \text{ ms}^{-1}$. The effect should also be detectable for WASP-177 and WASP-183 despite their more grazing transits, with an amplitude of $\sim 10 \text{ ms}^{-1}$.

5 CONCLUSIONS

We have presented the discovery of 3 transiting exoplanets from the WASP survey; WASP-177 b ($\sim 0.5 M_{\text{Jup}}$, $\sim 1.6 R_{\text{Jup}}$), WASP-181 b ($\sim 0.3 M_{\text{Jup}}$, $\sim 1.2 R_{\text{Jup}}$), and WASP-183 b ($\sim 0.5 M_{\text{Jup}}$, $\sim 1.5 R_{\text{Jup}}$). They all occupy the upper region of the mass-radius distribution for hot gas-giant planets but do not present exceptional targets for transmission spectroscopy. However, regarding the investigation of system spin-orbit alignment they do occupy an under investigated range of a/R_* and so could act as good probes of tidal realignment time-scales.

ACKNOWLEDGEMENTS

We thank the Swiss National Science Foundation (SNSF) and the Geneva University for their continuous support to our planet search programs. This work has been in particular carried out in the frame of the National Centre for Competence in Research ‘PlanetS’ supported by the Swiss National Science Foundation (SNSF). WASP-South is hosted by the South African Astronomical Observatory and we are grateful for their ongoing support and assistance. Funding for WASP comes from consortium universities and from the UK’s Science and Technology Facilities Council. TRAPPIST is funded by the Belgian Fund for Scientific Research (Fond National de la Recherche Scientifique, FNRS) under the grant FRFC 2.5.594.09.F, with the participation of the Swiss National Science Foundation (SNF). MG is a F.R.S.-FNRS Senior Research Associate. The research leading to these results has received funding from the European Research Council under the FP/2007-2013 ERC Grant Agreement 336480, from the ARC grant for Concerted Research Actions financed by the Wallonia-Brussels Federation, from

the Balzan Foundation, and a grant from the Erasmus+ International Credit Mobility programme (K Barkaoui). We thank our anonymous reviewer for their comments which helped improve the clarity of the paper.

REFERENCES

- Albrecht S., et al., 2012, *ApJ*, **757**, 18
 Anderson D. R., et al., 2012, *MNRAS*, **422**, 1988
 Anderson D. R., et al., 2015a, *A&A*, **575**, A61
 Anderson D. R., et al., 2015b, *ApJ*, **800**, L9
 Anderson D. R., et al., 2017, *A&A*, **604**, A110
 Armitage P. J., 2013, *Astrophysics of Planet Formation*. Cambridge University Press
 Barkaoui K., et al., 2018, preprint, ([arXiv:1807.06548](#))
 Birkby J. L., de Kok R. J., Brogi M., de Mooij E. J. W., Schwarz H., Albrecht S., Snellen I. A. G., 2013, *MNRAS*, **436**, L35
 Blanco-Cuaresma S., Soubiran C., Jofré P., Heiter U., 2014a, *A&A*, **566**, A98
 Blanco-Cuaresma S., Soubiran C., Heiter U., Jofré P., 2014b, *A&A*, **569**, A111
 Blanco-Cuaresma S., et al., 2016, in 19th Cambridge Workshop on Cool Stars, Stellar Systems, and the Sun (CS19). p. 22, [doi:10.5281/zenodo.155115](#)
 Blanco-Cuaresma S., et al., 2017, in Highlights on Spanish Astrophysics IX. pp 334–337
 Brogi M., de Kok R. J., Albrecht S., Snellen I. A. G., Birkby J. L., Schwarz H., 2016, *ApJ*, **817**, 106
 Claret A., 2000, *A&A*, **363**, 1081
 Claret A., 2004, *A&A*, **428**, 1001
 Collier Cameron A., et al., 2006, *MNRAS*, **373**, 799
 Collier Cameron A., et al., 2007, *MNRAS*, **380**, 1230
 Dai F., Winn J. N., 2017, *AJ*, **153**, 205
 Doyle A. P., Davies G. R., Smalley B., Chaplin W. J., Elsworth Y., 2014, *MNRAS*, **444**, 3592
 Fabrycky D., Tremaine S., 2007, *ApJ*, **669**, 1298
 Gaia Collaboration et al., 2016, *A&A*, **595**, A1
 Gaia Collaboration et al., 2018, *A&A*, **616**, A1
 Giles H. A. C., et al., 2018a, *MNRAS*, **475**, 1809
 Giles H. A. C., et al., 2018b, *A&A*, **615**, L13
 Gillon M., et al., 2011, *A&A*, **533**, A88
 Gillon M., et al., 2017, *Nature*, **542**, 456
 Goldreich P., Tremaine S., 1980, *ApJ*, **241**, 425
 Gray D. F., 2008, *The Observation and Analysis of Stellar Photospheres*. Cambridge University Press
 Gray R. O., Corbally C. J., 1994, *AJ*, **107**, 742
 Gustafsson B., Edvardsson B., Eriksson K., Jørgensen U. G., Nordlund Å., Plez B., 2008, *A&A*, **486**, 951
 Heiter U., Jofré P., Gustafsson B., Korn A. J., Soubiran C., Thévenin F., 2015, *A&A*, **582**, A49
 Hoeijmakers H. J., et al., 2018, *Nature*, **560**, 453
 Jehin E., et al., 2011, *The Messenger*, **145**, 2
 Jofré P., et al., 2014, *A&A*, **564**, A133
 Kreidberg L., et al., 2014, *ApJ*, **793**, L27
 Kreidberg L., et al., 2015, *ApJ*, **814**, 66
 Kupka F., Dubernet M. L., VAMDC Collaboration 2011, *Baltic Astronomy*, **20**, 503
 Lendl M., et al., 2012, *A&A*, **544**, A72
 Lendl M., et al., 2014, *A&A*, **568**, A81
 Lendl M., Cubillos P. E., Hagelberg J., Müller A., Juvan I., Fossati L., 2017, *A&A*, **606**, A18
 Luri X., et al., 2018, *A&A*, **616**, A9
 Mandel K., Agol E., 2002, *ApJ*, **580**, L171
 Marzari F., Nelson A. F., 2009, *ApJ*, **705**, 1575
 Maxted P. F. L., et al., 2011, *PASP*, **123**, 547
 Maxted P. F. L., Serenelli A. M., Southworth J., 2015, *A&A*, **575**, A36

Mazeh T., Perets H. B., McQuillan A., Goldstein E. S., 2015, *ApJ*, 801, 3
 McLaughlin D. B., 1924, *ApJ*, 60
 Pinsonneault M. H., DePoy D. L., Coffee M., 2001, *ApJ*, 556, L59
 Pollacco D. L., et al., 2006, *PASP*, 118, 1407
 Queloz D., et al., 2000, *A&A*, 354, 99
 Rasio F. A., Ford E. B., 1996, *Science*, 274, 954
 Rossiter R. A., 1924, *ApJ*, 60
 Schlafly E. F., Finkbeiner D. P., 2011, *ApJ*, 737, 103
 Sedaghati E., et al., 2017, *Nature*, 549, 238
 Southworth J., 2011, *MNRAS*, 417, 2166
 Spada F., Demarque P., Kim Y. C., Sills A., 2013, *ApJ*, 776, 87
 Stassun K. G., Torres G., 2018, *ApJ*, 862, 61
 Triaud A. H. M. J., et al., 2010, *A&A*, 524, A25
 Weidenschilling S. J., Marzari F., 1996, *Nature*, 384, 619
 Wu Y., Murray N., 2003, *ApJ*, 589, 605
 Wytttenbach A., et al., 2017, *A&A*, 602, A36
 Xiang-Gruess M., Kroupa P., 2017, *MNRAS*, 471, 2334
 de Kok R. J., Brogi M., Snellen I. A. G., Birkby J., Albrecht S., de Mooij E. J. W., 2013, *A&A*, 554, A82

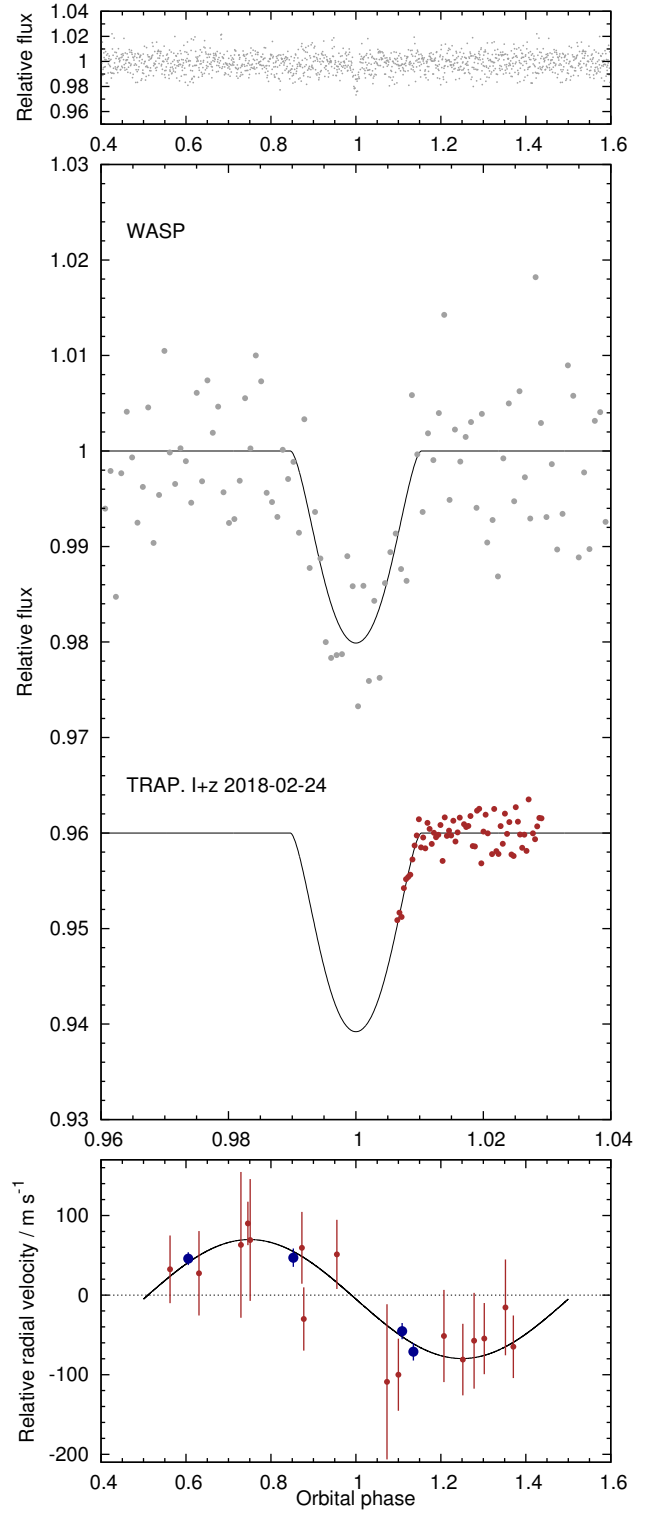


Figure 2. As for Fig.1 for the WASP-183 system.

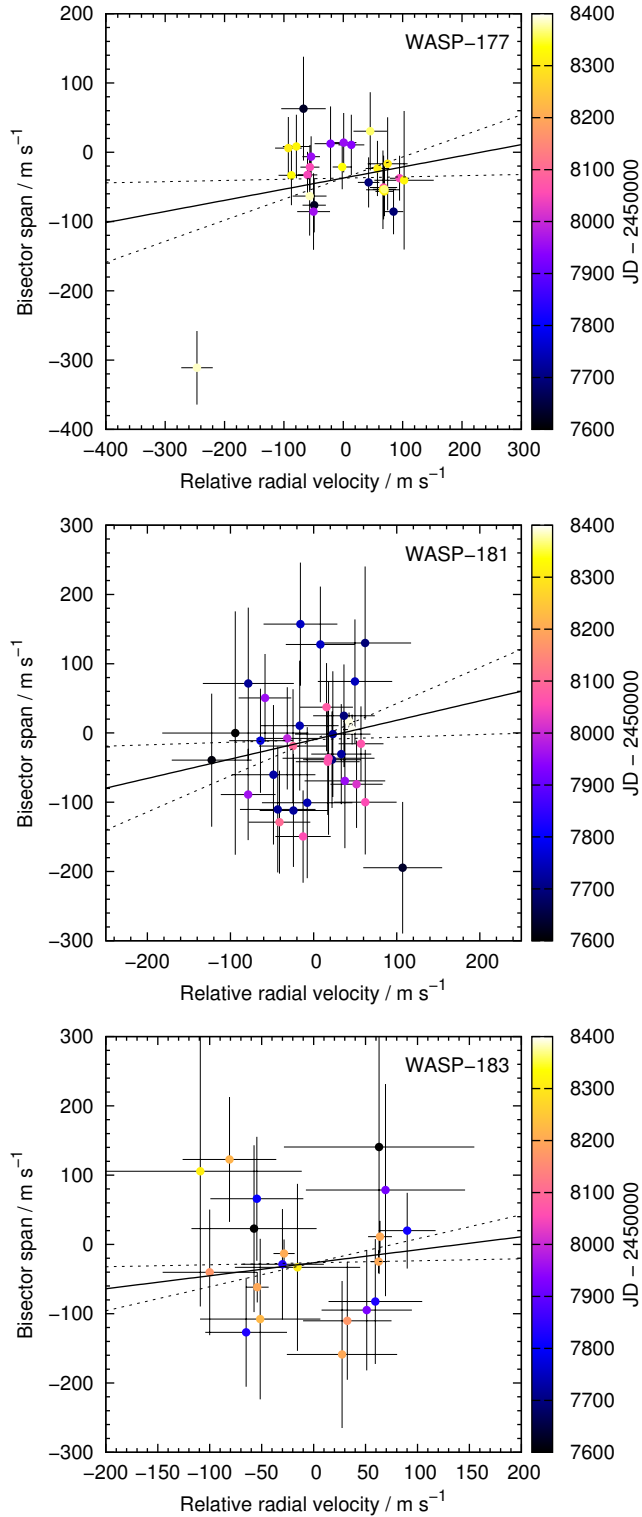


Figure 3. Radial velocity measurements plotted against line bisector spans. There is no strong correlation between the two, thus ruling out transit mimics. Solid lines are the linear best fit to the data. The dotted lines show the 1σ uncertainty limits on the fit.

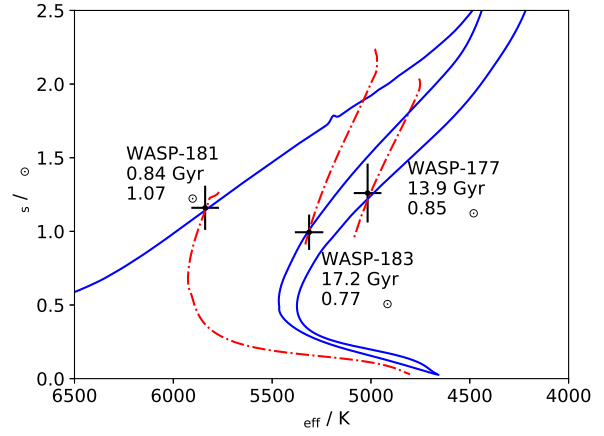


Figure 4. Isochrones (solid/blue) and evolution tracks (dot-dashed/red) output by BAGEMASS for each of the planets we present with the corresponding isochrone age and mass (labelled).

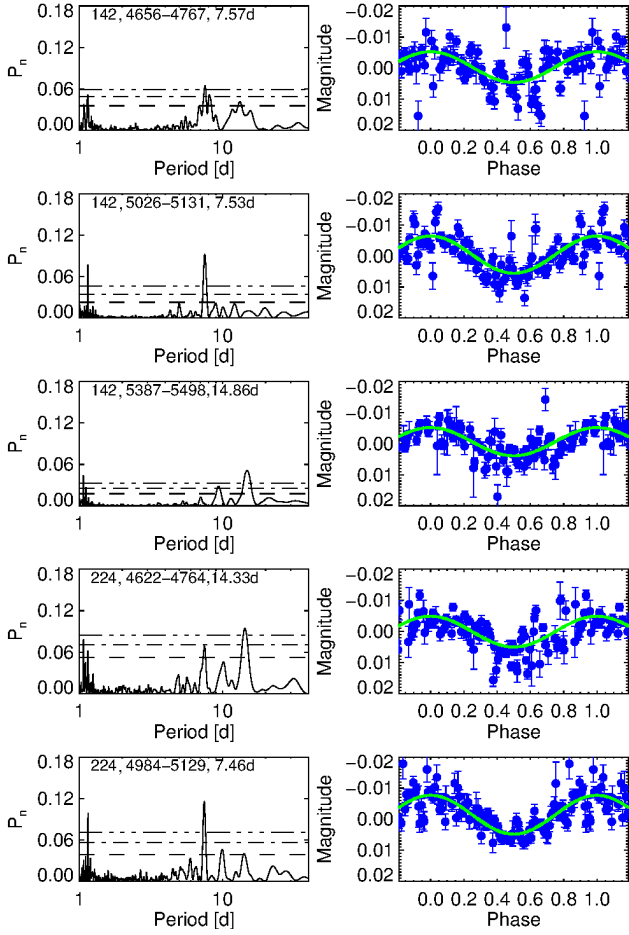


Figure 5. *Left:* Periodograms of the WASP lightcurves of WASP-177. Each is labeled with the corresponding camera ID, dates of the observation period (in JD-2450000) and period of the most significant signal. Horizontal lines indicate false-alarm probability levels of 0.1, 0.01 and 0.001. *Right:* Lightcurves folded on the most significant detected period.

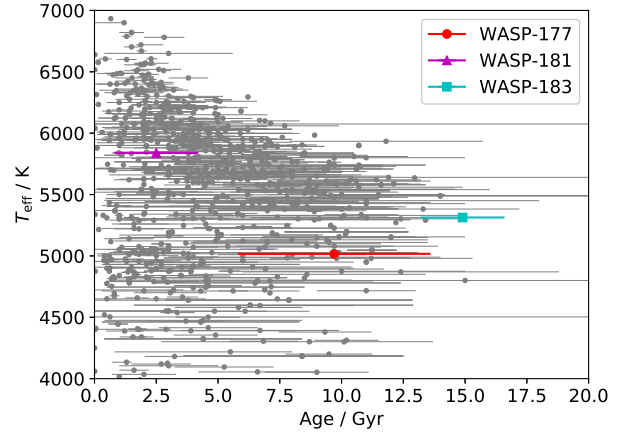


Figure 6. Age distribution for known exoplanet hosts with published uncertainties (grey) and planets presented in this paper (see legend). WASP-183 appears to be particularly old amongst planet hosts. However, we note it is unphysically old and so caution that this determination may be in part due to the K-dwarf radius anomaly. (Data from exoplanet.eu.)

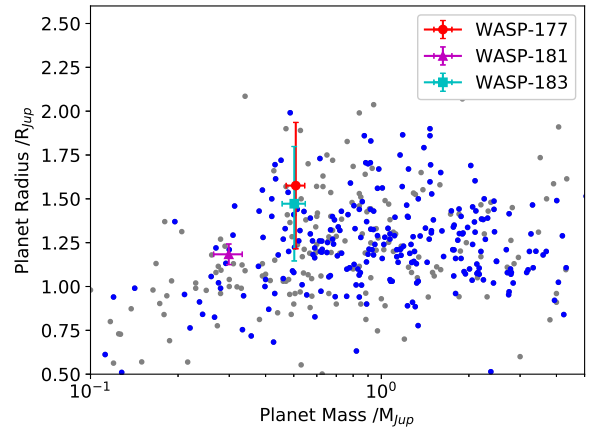


Figure 7. Mass-radius distribution for transiting planets. planets with masses determined to better than 10% precision are plotted in blue, otherwise the symbols are gray. WASP-177 b, WASP-181 b and WASP-183 b have been plotted with their error bars. Each is close to the upper most part of the distribution. WASP-177 b is in an area particularly sparsely populated by planets with well determined masses. (Prepared using data collated the TEP-Cat.)

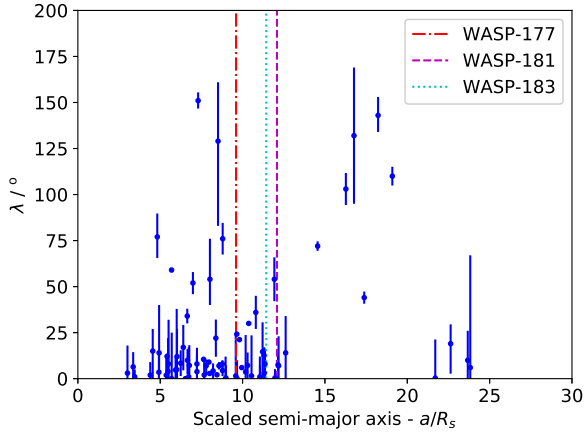


Figure 8. Distribution of planets with measured spin-orbit angles with cool host stars. WASP-177, WASP-181 and WASP-183 are all cool stars by this definition and the planets lie in the region where mis-alignment is often said to become more common. WASP-177 shows signs of being misaligned and so may be an interesting diagnostic in this region.

Table A1. Data from WASP

BJD -2450000	Diff. magnitude	Mag. error	Target
5026.54902768	-0.00254900	0.01949100	WASP-177
5026.54946749	0.02243000	0.01957700	WASP-177
5026.55550916	-0.00315500	0.01926500	WASP-177
5026.55596055	-0.00210900	0.01891800	WASP-177
5026.56091425	0.02301800	0.01892700	WASP-177
5026.56135407	-0.01070600	0.01829000	WASP-177
5026.56629620	-0.01820900	0.01836500	WASP-177
5026.56673601	-0.03087100	0.01769000	WASP-177
5026.57268508	-0.02453400	0.01780000	WASP-177
5026.57312490	-0.00700800	0.01818600	WASP-177

Table A2. Data from Trappist

BJD -2450000	Dif. Mag.	Mag. error	Filter	Target
7960.51599185	-0.00760377	-0.00345472	I+z	WASP-177
7960.51636185	-0.00029799	-0.00344426	I+z	WASP-177
7960.51664185	0.00210904	-0.00344268	I+z	WASP-177
7960.51691185	-0.00560489	-0.00344076	I+z	WASP-177
7960.51718185	-0.00165321	-0.00342985	I+z	WASP-177
7960.51754185	-0.00448940	-0.00342637	I+z	WASP-177
7960.51782185	-0.00682232	-0.00342797	I+z	WASP-177
7960.51809185	0.00938183	-0.00343320	I+z	WASP-177
7960.51836185	-0.00237813	-0.00343161	I+z	WASP-177
7960.51863185	-0.00132194	-0.00342244	I+z	WASP-177

Table A3. RV data

JD -2450000	RV (km/s)	RV error (km/s)	Instrument	Target
7626.633110	-7.19243	0.01963	CORALIE	WASP-177
7629.687997	-7.21044	0.03748	CORALIE	WASP-177
7689.581199	-7.05873	0.01634	CORALIE	WASP-177
7695.567558	-7.10068	0.01812	CORALIE	WASP-177
7933.845373	-7.16482	0.02686	CORALIE	WASP-177
7937.771917	-7.12978	0.02180	CORALIE	WASP-177
7952.880188	-7.14280	0.02144	CORALIE	WASP-177
7954.787481	-7.19749	0.01473	CORALIE	WASP-177
7961.703754	-7.19347	0.02763	CORALIE	WASP-177
8047.604223	-7.20369	0.01660	CORALIE	WASP-177

We include the data we used in this paper as online material. Examples of the tables are show here.

APPENDIX A: ONLINE DATA

This paper has been typeset from a $\text{\TeX}/\text{\LaTeX}$ file prepared by the author.

Table A4. Data from Euler

BJD - 2450000	Dif. Mag.	Mag. error	X-pos (pix)	Y-pos (pix)	Airmass	FWHM (pix)	Sky Bkg.	Exp. time (s)	Filter (days)	Object
8046.53876846	0.00034578	0.00359381	1070.950	571.822	1.1298	9.369	0.869	110	B	WASP-177
8046.54029585	0.00037222	0.00358208	1086.396	562.842	1.1289	7.076	0.903	110	B	WASP-177
8046.54281198	-0.8042	0.00213508	1085.203	562.140	1.1279	7.496	2.5836	300	B	WASP-177
8046.54652188	-0.00024034	0.00213411	1086.544	558.005	1.1267	7.632	2.4149	300	B	WASP-177
8046.55014519	0.00031779	0.00213539	1086.429	558.463	1.1262	7.980	2.3836	300	B	WASP-177
8046.55443872	0.00313122	0.00184258	1085.948	555.787	1.1264	7.832	3.2365	400	B	WASP-177
8046.55920903	0.00363211	0.00184463	1084.985	556.119	1.1274	7.832	3.4133	400	B	WASP-177
8046.56407976	0.00279818	0.00185139	1087.955	557.254	1.1296	7.928	3.4343	400	B	WASP-177
8046.56884813	0.00639643	0.00186126	1087.783	558.089	1.1326	9.099	3.9564	400	B	WASP-177
8046.57371742	0.00938502	0.00185610	1089.022	557.002	1.1369	7.880	3.5795	400	B	WASP-177